# Effect of Layer-Dependent Adatom Mobilities in Heteroepitaxial Metal Film Growth: Ni/Ru(0001)

J. A. Meyer, P. Schmid, and R. J. Behm
*Abteilung Oberflächenchemie und Katalyse, Universität Ulm, D-89069 Ulm, Germany*
(Received 7 October 1994)

Scanning tunneling microscopy observations show that (i) the lattice mismatch between Ni and Ru leads to a sequence of increasingly relaxed structures in Ni films grown on Ru(0001), and (ii) the density of Ni islands changes drastically with the thickness of the underlying Ni film. The latter is associated with an increase in Ni mobility; from monolayer to three-layer Ni films a reduction in Ni adatom diffusion barrier of 300 meV is estimated. Such effects are shown to significantly affect film growth and, in this case, to promote smoother growth. New possibilities for obtaining smoother film growth for heteroepitaxial systems, in general, are discussed.

PACS numbers: 68.55.–a, 61.16.Ch

Epitaxial growth affords the opportunity to make materials with morphologies and chemical compositions which would not ordinarily occur in nature [1–4]. By varying the experimental parameters of temperature, deposition rate, and, more recently, additive (surfactant) concentrations the characteristics of the growing film can be controlled to a certain extent [5–12]. For heteroepitaxy further effects come into play, namely, the change in film structure due to the removal of strain, and the change in electronic properties with increasing film thickness. The strain results from the lattice mismatch between the substrate and the growing film. In this Letter we demonstrate that these surface modifications can have a drastic effect on the adatom mobilities, leading to layer-dependent island densities. The structure of and adatom mobilities on films of different layer thicknesses were determined by scanning tunneling microscopy (STM). For these experiments we first prepared well-defined Ni films on a Ru(0001) substrate by deposition at 550 K. This temperature is sufficiently high to produce well-ordered surfaces and rather large terraces, but not high enough to create the equilibrium morphology of that system, which consists of 3D crystallites growing on a single Ni layer (Stranski-Krastanov growth) and which is obtained after deposition at or annealing to higher temperatures [13,14]. On these thin film substrates we subsequently deposited small amounts of Ni in a second dose at room temperature. From the distribution and density of the Ni islands obtained after the second dose we gain insight into adatom diffusion on and among the various well-defined Ni layers. The results lead us to introduce layer dependent mobilities and island densities as a general concept for heteroepitaxy with substantial implications for growth descriptions and film morphologies.

Deposition and STM imaging were carried out at $p < 3 \times 10^{-8}$ Pa, on carefully cleaned Ru(0001) substrates. Further details on the experimental setup and procedures and on the growth behavior of that system will be described elsewhere [14]. STM images were recorded in a pocket-sized STM at tunnel currents around 1 nA and bias voltages of 100 mV. The images are presented in either a top view representation, with darker areas corresponding to lower levels, or in a bird's eye view with illumination from the left hand side.

For the experiments described here we start with annealed Ni films of nominally 0.3, 1.3, and 2.5 monolayer (ML) coverage, with local film thicknesses between zero and four Ni layers. As mentioned recently, the pseudomorphic Ni layer is stable only in the submonolayer regime [14]. After completion of the first monolayer, incorporation of additional Ni adatoms leads to a reconstruction of that layer to form a denser phase with a periodic arrangement of triangular domain boundaries between fcc and hcp areas. This structure is shown in Fig. 1(a). The white lines represent Ni atoms located on slightly higher bridge sites, while in the other areas the Ni atoms reside on lower fcc and hcp-type threefold hollow sites. Similar structures had been observed for Cu films on Ru(0001) [15] and on homoepitaxial Pt(111) surfaces [16]. For bilayer and thicker films, hexagonal Moiré structures are formed [Figs. 1(b) and 1(c). The atomic spacings of 2.5 Å, the distance between the long-range corrugation maxima of 32 Å, and the fact that these maxima are oriented along atomic rows all agree with a model where a nondistorted hexagonal Ni lattice (nearest neighbor distance 2.49 Å) is stacked on top of the substrate (nearest neighbor distance 2.7 Å). The amplitude of the corrugation decays steadily with increasing film thickness until after ten layers at which point this modulation is no longer visible and the surface has largely adopted the Ni(111) structure. Simultaneously, the height difference at Ru(0001) substrate steps between the $n$th layer on an upper terrace and the $(n + 1)$th layer on a lower terrace decreases steadily with increasing Ni thickness; for $n = 0$, this is ~0.5 Å, and after ten layers the height difference is no longer detectable.

Nucleation and growth of Ni islands after deposition at 300 K (flux 0.3 ML/min.) on predeposited Ni films is illustrated in the images in Fig. 2. For 0.3 ML predeposition at 550 K all Ni is condensed at Ru(0001) steps and pseudomorphic to the substrate, leaving large areas of the

 0031-9007/95/74(19)/3864(4)$06.00 

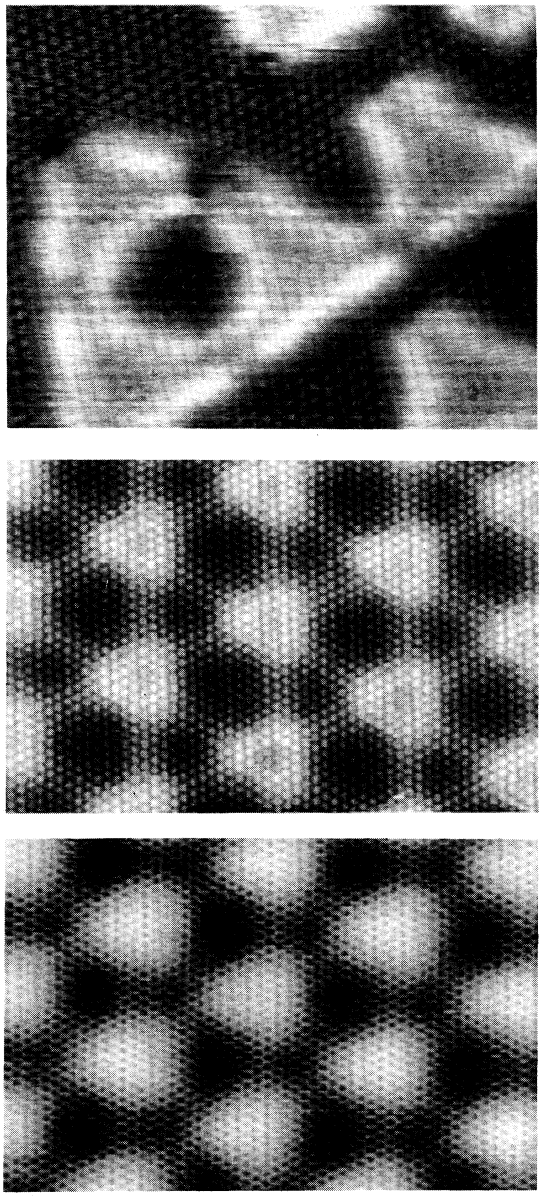


FIG. 1. High resolution STM images resolving the atomic structure and long-range modulation of thin Ni films on Ru(0001). (a) Reconstructed monolayer area in a film with >1 ML coverage, with triangular-shaped domain boundaries between fcc and hcp areas (8 nm × 6 nm). (b) Isotropically contracted, approximately hexagonal structure of a Ni film of three layer thickness (10 nm × 7 nm). (c) Uniformly contracted, hexagonal structure of a Ni film of five layer thickness (10 nm × 7 nm).

surface uncovered [Fig. 2(a)]. In this figure the Ni areas are identified by their rough edge to the underlying Ru terrace and the smooth transition line to the edge of the adjoining next higher Ru terrace ($\Delta z = 0.5$ Å). Following a second Ni dose of 0.05 ML at room temperature, we now find a number of small new Ni islands. On the bare surface areas the island density ($\sim 5 \times 10^{10}$ /cm$^2$) and roughly hexagonal shape are similar to those observed after room temperature deposition on the clean substrate. While these islands are generally homogeneously distributed, there is an increased Ni island density on the Ru side of the Ru-Ni interface at Ru substrate steps, indicating an attractive potential in this region. Furthermore, the edges of the original Ni islands have roughened by condensation of postdeposited Ni adatoms. The roughness occurs because of the lower mobility of Ni adatoms along the step edge at 300 K. We also find a few small Ni islands on the large, predeposited Ni areas along step edges. Less extended first layer Ni regions are often free of second layer Ni islands. Clearly, the total coverage of second layer Ni is much smaller than the coverage of new Ni islands on the Ru terraces. This indicates that most Ni atoms impinging on the first layer Ni areas could migrate to and pass the island edges, either to the neighboring Ru terrace or by dropping over the Ni island edge. These atoms are then trapped at the ascending Ni step. Simultaneously with the formation of second layer Ni islands, the first layer superstructure, indicative of denser Ni packing [as shown in Fig. 1(a)], is seen to develop in the central area of larger first layer Ni islands, while the remaining parts at the perimeter of the islands are still pseudomorphic to the substrate [Fig. 2(a)].

Deposition of 0.05 ML of Ni at room temperature on a 550 K predeposited 1.3 ML Ni film yields a surface, as shown in Fig. 2(b). It should be noted that, in this case, the first layer Ni was not pseudomorphic but already displayed the reconstructed, more densely packed superstructure before postdeposition and that the second layer also exhibited its characteristic quasihexagonal structure. The most striking feature in this image is that the density of Ni islands on the reconstructed first layer Ni areas is a factor of ~25 higher than on the pseudomorphic first layer Ni shown in Fig. 2(a). These islands often show an ordered arrangement with island-island spacings of about 25 Å, similar to the periodicity of the reconstruction. Hence, this must be attributed to preferential nucleation induced by the reconstruction of the underlying layer, as has been previously observed for Ni on Au(111) [17]. The density of Ni islands on the second Ni layer areas, which stretch along ascending Ru substrate steps, is significantly smaller than on the reconstructed first layer by about a factor of 6. The difference in density between these two Ni layers is also clearly seen in Fig. 2(c). The transition between monolayer Ni areas (on the upper Ru terrace) and bilayer Ni areas (on the lower Ru terrace) at Ru steps is marked by a dense line of Ni islands, i.e., there is preferential nucleation of Ni islands at these sites [Figs. 2(b) and 2(c)].

The image in Fig. 2(c), recorded after predeposition of 2.5 ML of Ni film at 550 K and subsequent dosing with 0.05 ML of Ni at room temperature, dramatically illustrates the drastically different island densities and sizes on the various Ni layers up to the fourth layer. The region between the black arrows represents a single

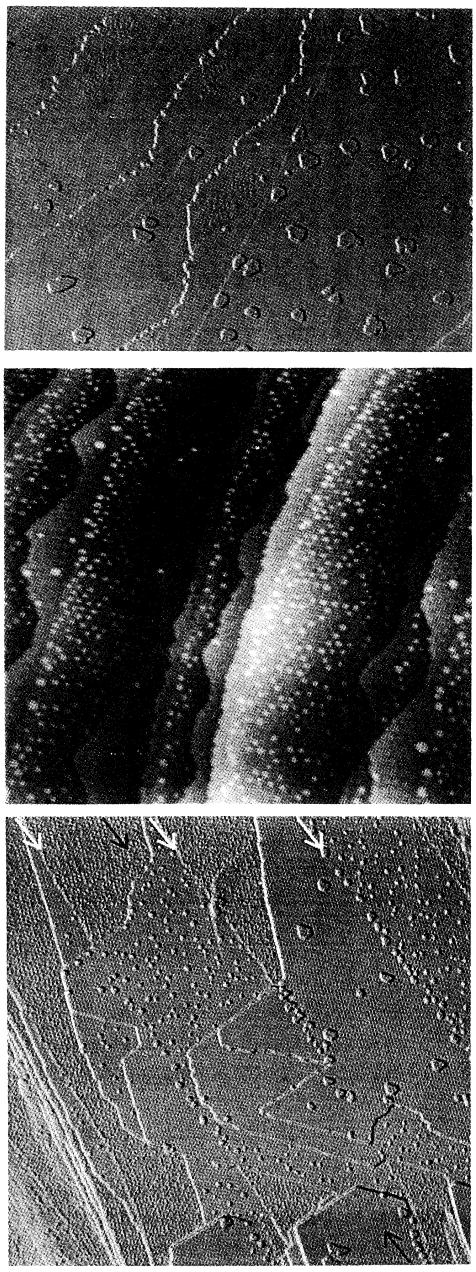

FIG. 2. Large scale images of Ni covered Ru(0001) surfaces after predeposition of 0.3 (a), 1.3 (b), and 2.5 ML (c) at 550 K and postdeposition of small amounts of Ni at room temperature. (a) Postdeposited small Ni islands on the substrate and first layer Ni islands condensed at Ru step edges (310 nm × 250 nm); (b) postdeposited Ni islands on monolayer and bilayer Ni regions (140 nm × 140 nm); (c) postdeposited Ni islands on Ni films of local thickness from one to four layers. The long-range modulation of the films is resolved. Underlying Ru step edges are marked by white arrows (400 nm × 400 nm).

Ru(0001) terrace. Moving from top to bottom on a line between these arrows the following Ni film layers are observed 1, 2, 4, 3, 4, 3, 2, and 4, each layer with its characteristic structure and island density. Additionally, the step edges of the underlying substrate (three of which are marked with white arrows in the image) display a very high island density; they are decorated with Ni islands. It should also be noted that the larger islands formed during the room temperature dose immediately display the characteristic structure and preferential edge orientations of their respective layers.

The Ni island densities on the different Ni film thicknesses for this system change by a factor of 65 in moving from monolayer to three-layer Ni areas. The island density on the fourth layer is already too small to be evaluated on this surface. Hence the island density decays steadily to larger film thicknesses. The island density on the pseudomorphic Ni monolayer [compare Figs. 2(a) and 2(b)] is anomalously small. This may be caused not only by a higher adatom mobility but also in part by a reduction in second layer adatom density due to incorporation of these adatoms into the first Ni layer during the reconstruction [14]. Here we shall concentrate on the nonpseudomorphic Ni layers. If we assume that the Ni-Ni bonding in the adatom cluster formed during nucleation, i.e., the cluster binding energy [18,19], does not change much with the number of underlying Ni layers, then the change in island density can be interpreted as being due to a change in Ni adatom mobility. If, for a rough estimate, we assume a critical island size of one for Ni nucleation and apply the usual functional form for the island density $N$ as a function of diffusion rate and hopping rate, we obtain

$$N \approx \left(\frac{r}{h}\right)^{0.3},$$

where $h$ is the diffusion rate, and $r$ is the deposition rate. This yields a decrease in the Ni diffusion barrier of 300 meV from monolayer to three layer Ni films [18,19].

This observed change in adatom mobility with increasing Ni layer thickness has a drastic effect on the growth process and the resulting film morphology. In the present case, with a decreasing island density or increasing adatom mobility for increasing film thicknesses, interlayer transport will be favored, and smoother morphologies will result. That this should be the case is intuitively clear: A higher mobility on top of islands will increase the attempt frequency to move off of the islands and thus increase interlayer transport. This is confirmed by a model of kinetically limited film growth. Using steady state approximations and assuming circular islands, the smoothness of a film is calculated as a function of the various diffusion barriers on the surface. Full details will be published shortly [20]. The result of importance here is that the smoothness of a growing film can be described by the relation

$$\left(\frac{R_0}{R_1}\right)^2 = \frac{h_0}{h_1} + \frac{2h_0}{R_1 s} \equiv \gamma,$$

where $h_0$ and $h_1$ are the adatom hopping frequencies on the $n$th and $(n+1)$th layer, respectively, $R_0$ is a measure of spacing between islands on the $n$th layer, $R_1$ is the radius of the $n$th layer island, which supports nucleation

of $(n + 1)$th layer islands, $s$ is the barrier for moving over a descending step edge, and $\gamma$ is a measure of smoothness. A lower value of $\gamma$ indicates a smoother film. An increasing mobility on higher layers gives $h_0 < h_1$ and, as expected, a smaller value of $\gamma$ as compared to $h_0 = h_1$. If the step edge barrier is not too large, this gives layer growth, and only for rather large values of $s$ (considerably larger than for the case $h_0 = h_1$) will kinetically limited multilayer growth with many layers exposed simultaneously result.

The nucleation of the Ni islands shown in Figs. 2(a)–2(c) is also strongly influenced by the presence of steps in the underlying Ru substrate. This effect is already seen in the substrate-to-Ni monolayer layer transition in Fig. 2(a). The Ru step edges continue to serve as nucleation centers for Ni islands for higher Ni layers. As seen in Fig. 2(c), each Ru step is marked by a row of Ni islands. For the Ni terrace sizes obtained in this study, nucleation at these boundaries dominates the growth process for the fifth and higher Ni layers, i.e., there is no homogeneous nucleation seen in these Ni layers.

The reason for the changing Ni mobility with layer height is not clear. It may be due to electronic effects arising from contributions from the substrate. However, given the observation of nucleation at specific sites in the first Ni layer, we feel a much more likely cause for the change in Ni mobility are structural changes in the growing film, due to and accompanying the successive relaxation of lattice strain. This leads to local inhomogeneities in these surfaces, such as Ni atoms on bridge sites in the domain boundaries of the reconstructed monolayer film, which provide slightly different adsorption sites for next layer adatoms. Independent of whether these sites are more or less favorable than others, this will result in an effective slowdown of the adatoms. This slowdown should become smaller and smaller as the surface becomes more homogeneous, in agreement with our structural observation for Ni/Ru(0001), where for increasing film thickness the surface indeed becomes more and more homogeneous (see the atomic structures in Fig. 1).

Observations of the underlying film thickness affecting the adatom mobilities for the Ni/Ru(0001) system have broader implications for the heteroepitaxial film growth, in particular, for the growth of ultra thin films of only a few layers' thickness (for thick films this effect plays no role, since the adatom mobilities are expected to have saturated). Under favorable conditions, e.g., increasing structural homogeneity of the film, kinetically limited layer growth and hence smooth surface morphologies can be facilitated. In contrast to other ways of promoting layer growth such as varying the temperature or the rate during growth [21,22], briefly sputtering between deposition of individual layers to enhance island nucleation [22], or adding surfactants to enhance interlayer transport [5–12], this effect is intrinsic to the respective film system. These ideas are expected to be applicable in the choice of buffer layers, where materials with a slight mismatch might promote layer growth of the deposit better than materials optimized for minimal mismatch.

In summary we have identified a pronounced effect of the underlying film thickness on the density of adislands in Ni/Ru(0001), accompanying a change in surface structure of the respective films to accommodate the lattice mismatch. We attribute this to a steady increase of the adatom mobility on these films with increasing thickness and increasing film homogeneity. Making usual assumptions for the critical island size we estimate the reduction in the Ni diffusion barrier from second to fourth layer adatoms to be around 300 meV. Additionally, the underlying step edges in the substrate were shown to act as preferential nucleation sites. Similar effects are generally expected to occur in general for heteroepitaxy; the implications for smoother growth are commented upon. Further theoretical work is required to elucidate the specific physical origin for the observed change in diffusivity.

We gratefully acknowledge support from the Alexander-von-Humboldt Foundation through a fellowship for J. A. M.

[1] C. Günther *et al.,* Ber. Bunsen-Ges. Phys. Chem. **97**, 522 (1993).
[2] S.-L. Chang and P. A. Thiel, CRC Crit. Rev. Surf. Chem. **3(3/4)**, 239 (1994).
[3] M. T. Keif and W. F. Egelhoff, Jr., Phys. Rev. B **47**, 10785 (1993), and references therein.
[4] *Kinetics of Ordering and Growth at Surfaces,* edited by M. G. Lagally (Plenum, New York, 1990).
[5] M. Horn-von Hoegen *et al.,* Phys. Rev. Lett. **67**, 1130 (1991).
[6] M. Schmidt, H. Wolter, and K. Wandelt, Surf. Sci. **307**, 507 (1994).
[7] H. Wolter, M. Schmidt, and K. Wandelt, Surf. Sci. **298**, 173 (1993).
[8] M. Copel *et al.,* Phys. Rev. Lett. **63**, 632 (1989).
[9] W. F. Egelhoff, Jr. and D. A. Steigerwald, J. Vac. Sci. Technol. A **7**, 2167 (1989).
[10] H. L. Gaigher, N. G. van der Berg, and J. B. Malherbe, Thin Solid Films **137**, 337 (1986).
[11] H. A. van der Vegt *et al.,* Phys. Rev. Lett. **68**, 3335 (1992).
[12] J. Vrijmoeth *et al.,* Phys. Rev. Lett. **72**, 3843 (1994).
[13] P. J. Berlowitz *et al.,* Surf. Sci. **205**, 1 (1988).
[14] J. A. Meyer and R. J. Behm (to be published).
[15] G. Pötschke *et al.,* Surf. Sci. **251/252**, 592 (1991).
[16] M. Bott, Th. Michely, and G. Comsa, Phys. Rev. Lett. **70**, 1489 (1993).
[17] D. D. Chambliss, R. J. Wilson, and S. Chiang, Phys. Rev. Lett. **66**, 1721 (1991).
[18] J. A. Venables, G. D. Spiller, and M. Hanbücken, Rep. Prog. Phys. **47**, 399 (1984).
[19] M. C. Bartelt and J. W. Evans, Phys. Rev. B **46**, 12675 (1992).
[20] J. A. Meyer *et al.,* (to be published).
[21] V. A. Markov *et al.,* Surf. Sci. **250**, 229 (1991).
[22] G. Rosenfeld *et al.,* Phys. Rev. Lett. **71**, 895 (1993).

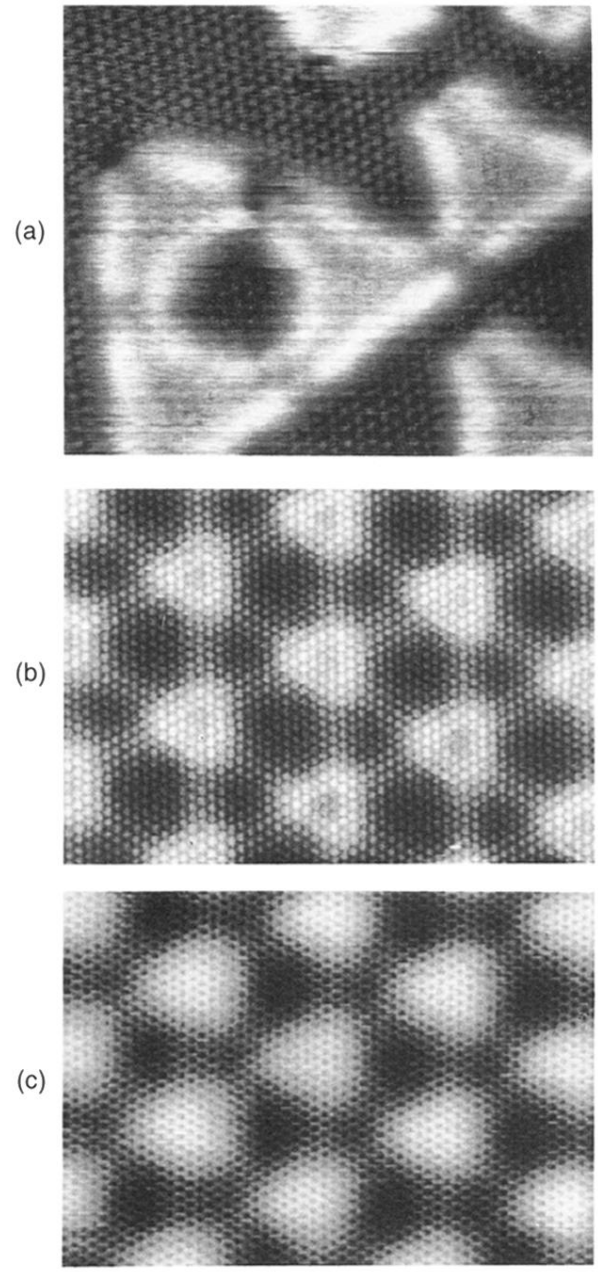


FIG. 1. High resolution STM images resolving the atomic structure and long-range modulation of thin Ni films on Ru(0001). (a) Reconstructed monolayer area in a film with $>1$ ML coverage, with triangular-shaped domain boundaries between fcc and hcp areas (8 nm $\times$ 6 nm). (b) Isotropically contracted, approximately hexagonal structure of a Ni film of three layer thickness (10 nm $\times$ 7 nm). (c) Uniformly contracted, hexagonal structure of a Ni film of five layer thickness (10 nm $\times$ 7 nm).

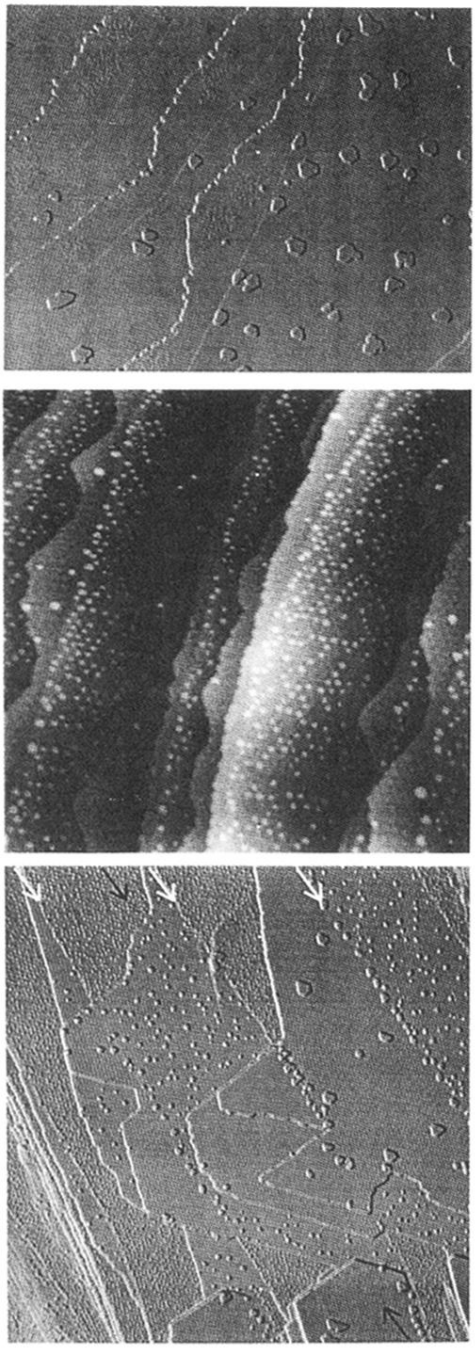

FIG. 2. Large scale images of Ni covered Ru(0001) surfaces after predeposition of 0.3 (a), 1.3 (b), and 2.5 ML (c) at 550 K and postdeposition of small amounts of Ni at room temperature. (a) Postdeposited small Ni islands on the substrate and first layer Ni islands condensed at Ru step edges (310 nm $\times$ 250 nm); (b) postdeposited Ni islands on monolayer and bilayer Ni regions (140 nm $\times$ 140 nm); (c) postdeposited Ni islands on Ni films of local thickness from one to four layers. The long-range modulation of the films is resolved. Underlying Ru step edges are marked by white arrows (400 nm $\times$ 400 nm).